# Bisurea-Based Supramolecular Polymers for Tunable Biomaterials

DOI:
[10.1002/chem.202303361](10.1002/chem.202303361)

Document status and date:
Published: 26/01/2024

Document Version:
Publisher's PDF, also known as Version of Record (includes final page, issue and volume numbers)

Please check the document version of this publication:

• A submitted manuscript is the version of the article upon submission and before peer-review. There can be important differences between the submitted version and the official published version of record. People interested in the research are advised to contact the author for the final version of the publication, or visit the DOI to the publisher's website.
• The final author version and the galley proof are versions of the publication after peer review.
• The final published version features the final layout of the paper including the volume, issue and page numbers.

[Link to publication](Link to publication)

Chemistry–A European Journal

Research Article
doi.org/10.1002/chem.202303361

Chemistry
Europe
European Chemical
Societies Publishing

www.chemeurj.org

*Hot Paper*

# Bisurea-Based Supramolecular Polymers for Tunable Biomaterials

Marle E. J. Vleugels,[a, d] Rik Bosman,[a, d] Piers H. da Camino Soligo,[a, d] Stefan Wijker,[a, d] Bence Fehér,[b, d] A. J. H. Spiering,[a, b, d] Laura Rijns,[c, d] Riccardo Bellan,[c, d] Patricia Y. W. Dankers,[c, d] and Anja R. A. Palmans*[a, d]

Water-soluble supramolecular polymers show great potential to develop dynamic biomaterials with tailored properties. Here, we elucidate the morphology, stability and dynamicity of supramolecular polymers derived from bisurea-based monomers. An accessible synthetic approach from 2,4-toluene diisocyanate (TDI) as the starting material is developed. TDI has two isocyanates that differ in intrinsic reactivity, which allows to obtain functional, desymmetrized monomers in a one-step procedure. We explore how the hydrophobic/hydrophilic ratio affects the properties of the formed supramolecular polymers by increasing the number of methylene units from 10 to 12 keeping the hydrophilic hexa(ethylene glycol) constant. All bisurea-based monomers form long, fibrous structures with 3–5 monomers in the cross-section in water, indicating a proper hydrophobic\hydrophilic balance. The stability of the supramolecular polymers increases with an increasing amount of methylene units, whereas the dynamic nature of the monomers decreases. The introduction of one Cy3 dye affords modified supramolecular monomers, which co-assemble with the unmodified monomers into fibrous structures. All systems show excellent water-compatibility and no toxicity for different cell-lines. Importantly, in cell culture media, the fibrous structures remain present, highlighting the stability of these supramolecular polymers in physiological conditions. The results obtained here motivate further investigation of these bisurea-based building blocks as dynamic biomaterial.

## Introduction

Supramolecular polymers are ubiquitous in nature and vital for biological systems. Natural supramolecular polymers fulfill a range of functions such as structural support, cell division and cell motility.[1–3] These natural supramolecular polymers are all stable, yet dynamic structures. The dynamicity in the structures arises from reversibility due to the weak noncovalent interactions between the building blocks. Although noncovalent interactions are weaker than covalent bonds, the combination of multiple inter- and intra-molecular noncovalent interactions can lead to robust yet dynamic structures that exhibit complex functions. Synthetic supramolecular polymers forming one-dimensional aggregates in solution have attracted considerable interest, as they mimic several of the properties of naturally occurring fibrils and open new avenues in terms of functionality.[4–9] Especially water-soluble supramolecular polymers are attractive candidates for functional assemblies in the field of biomaterials, due to their compatibility with natural systems.[10,11]

In addition to compatibility with natural systems, the modularity of supramolecular polymers is also an important property, as the noncovalent interactions between the monomers allow for easily accessible, tunable supramolecular polymers via copolymerization. This modularity has been employed in peptide amphiphiles where bone regeneration, stabilization of growth factors and nerve regeneration after spinal cord injury have been achieved.[12–14] Ureido-pyrimidinone (UPy) based polymers have also extensively been studied in biological environments. By mixing mono- and bivalent UPy monomers, polymers with tunable dynamics can be obtained.[15] Functionalization with charged moieties or peptides resulted in supramolecular polymers which showed siRNA delivery, cellular adhesion and antimicrobial activity.[16–18] A similarly well-studied supramolecular building block is the benzene-1,3,5-tricarboxamide (BTA), which forms fiber-like structures in water.[19–26] Recently, peripheral functional groups have been introduced into the BTA-based systems via co-assembly with functional

[a] Dr. M. E. J. Vleugels, R. Bosman, P. H. da Camino Soligo, S. Wijker,
A. J. H. Spiering, Prof. Dr. A. R. A. Palmans
Laboratory of Macromolecular and Organic Chemistry
Department of Chemical Engineering and Chemistry
Eindhoven University of Technology, Eindhoven (The Netherlands)
E-mail: a.palmans@tue.nl

[b] Dr. B. Fehér, A. J. H. Spiering
Laboratory of Self-Organizing Soft Matter
Department of Chemical Engineering and Chemistry
Eindhoven University of Technology, Eindhoven (The Netherlands)

[c] Dr. L. Rijns, R. Bellan, Prof. Dr. P. Y. W. Dankers
Laboratory of Chemical Biology
Department of Biomedical Engineering
Eindhoven University of Technology, Eindhoven (The Netherlands)

[d] Dr. M. E. J. Vleugels, R. Bosman, P. H. da Camino Soligo, S. Wijker,
Dr. B. Fehér, A. J. H. Spiering, Dr. L. Rijns, R. Bellan, Prof. Dr. P. Y. W. Dankers,
Prof. Dr. A. R. A. Palmans
Institute for Complex Molecular Systems
Eindhoven University of Technology, Eindhoven (The Netherlands)

*Chem. Eur. J.* 2024, 30, e202303361 (1 of 10)

© 2023 The Authors. Chemistry - A European Journal published by Wiley-VCH GmbH

**Chemistry–A European Journal**

Research Article
doi.org/10.1002/chem.202303361

**Chemistry
Europe**
European Chemical
Societies Publishing

monomers.[27,28] These examples showed the potential of BTAs as biomaterials, but also highlighted the need for desymmetrized monomers for optimal solubility and presentation of the functional groups. Since the *C₃*-symmetrical BTA molecules contain three reactive sites for the attachment of functional groups, the synthesis to obtain desymmetrized building blocks is lengthy, and overall yields are typically low. Starting from a desymmetrized precursor reduced the number of steps, but also reduced the water-solubility of the monomers.[29]

Another widely used supramolecular motif is the urea motif, which is synthetically readily accessible by the addition of amines to isocyanates. Compared to amides, ureas form stronger interactions due to multiple and cooperative hydrogen bonds.[30,31] The group of Sijbesma investigated the use of this motif to create water-compatible bolaamphiphiles for the design of supramolecular fibers, which showed strain-stiffening properties and bioactivity.[32–34] The group of Brendel has made use of this stronger interaction to drive the assembly of benzene trisureas into cylinder like objects in water, guided by strong hydrogen bonds rather than the hydrophobic/hydrophilic balance of the monomer.[30,31] Another synthetically readily accessible urea motif based on 2,4-toluene diisocyanate (TDI) was developed by the group of Bouteiller.[35,36] The bisurea 2,4-bis(2-ethylhexylureido)toluene (EHUT) was studied in great detail in organic media and was found to form long cylindrical structures due to self-association through hydrogen bonding of the ureas. TDI bears two reactive sites instead of three, making it an interesting molecule for desymmetrization with fewer synthetic steps. Desymmetrized ureido toluene (UT) based bisurea have been obtained by two-step reactions of TDI with distinct amines,[37] or via 2-methyl-5-nitroaniline as starting material.[38,39] Bouteiller and coworkers also reported water-compatible analogues, which formed supramolecular polymers in water.[40] Here, the combination of an alkyl spacer with a disperse oligo(ethylene glycol) of on average 7 units gave rise to water-compatible supramolecular polymers. In water, the monomers assembled into long fibers with multiple molecules in the cross section. The fiber formation was driven by directional hydrogen bonding in combination with hydrophobic interactions of the core.[40,41] These early studies highlighted the potential of the UT system in water, but the dynamicity of the fibers or biocompatibility was not within the scope of the research. Inspired by the work of Bouteiller, we explore the UT motif as a building block towards tunable supramolecular biomaterials and investigate desymmetrization of this building block to selectively introduce functional groups.

In this work, three new monomers based on the UT motif (**UT-C₁₀**, **UT-C₁₁** and **UT-C₁₂**) are prepared and the influence of the alkyl spacer length while keeping the length of the water-soluble part constant using discrete hexa(ethylene glycol) is systematically investigated. Discrete hexa(ethylene glycol) is selected based on exploratory studies we performed, which showed that the tetra(ethylene glycol) typically used in BTAs[19] did not provide sufficient water-solubility for the UT systems. We present a detailed investigation of the aqueous self-assembly of the monomers in water using spectroscopic studies and small angle neutron scattering techniques (SANS), as well

as cryogenic transmission electron microscopy (cryo-TEM). The dynamic exchange of the monomers between polymers is assessed with hydrogen/deuterium exchange followed by mass spectrometry (HDX-MS).[21] Furthermore, we report the synthesis of a desymmetrized UT building block, obtained from TDI in a 1-pot procedure with one cyanine dye (**UT-C₁₁-Cy3**). Finally, we take a first step in addressing the potential of the UT assemblies as biomaterials by co-assembling **UT-C₁₁-Cy3** with **UT-C₁₁** using fluorescence microscopy, and investigating the compatibility of the supramolecular polymers with two different human cell types and their stability in the presence of cell culture media.

## Results and Discussion

### Design and Synthesis

The monomer design is based on the well-studied bisurea motif developed by Bouteiller and coworkers.[36,40–42] Here, we include aliphatic chains to shield the hydrogen-bonding units from the surrounding aqueous solution and hexa(ethylene glycol) with alcohol end groups to provide solubility in water.[43] To investigate the influence of the alkyl spacer length on water-compatibility, chains with a length of 10, 11 or 12 methylene units were selected (Figure 1).

All monomers were obtained by reacting 2,4-toluene-diisocyanate with amine terminated benzyl protected alcohol side chains (Scheme 1A). The synthesis of amine-terminated side chains is based on literature procedures,[19,44] but starting from hexa(ethylene glycol) instead of the previously applied tetra(ethylene glycol). The latter provided insufficient water solubility for the UT system in exploratory studies (data not shown). Catalytic hydrogenation to deprotect the benzyl protected alcohols yielded **UT-C₁₀**, **UT-C₁₁** and **UT-C₁₂**. After careful analysis of the end-products, we noticed small amounts of the surfactant-like alkyl-hexa(ethylene glycol) (0.05–0.1 equiv.) (Scheme S1). This side product was traced back as a byproduct formed during the synthesis of the amine terminated side chains (for a detailed discussion, see the Supporting Information). While the alkyl-hexa(ethylene glycol) could not be removed using column chromatography, it will also not affect our subsequent studies: we recently showed for BTAs that low amounts of such surfactants below their critical micelle concentration, CMC, intercalate into the supramolecular polymers without disturbing their morphology.[45] Since the amount of the alkyl-hexa(ethylene glycol) is below 0.1 equiv., the structure and morphology of the supramolecular assemblies will not be affected.
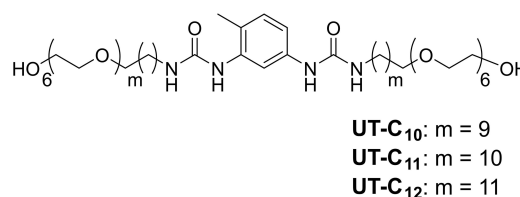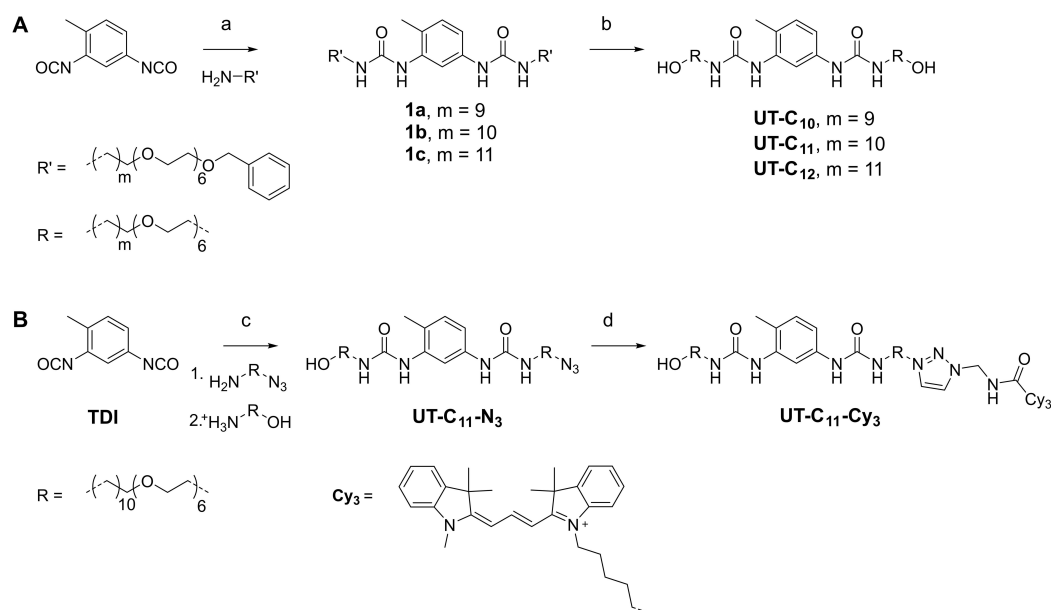


**UT-C₁₀**: m = 9
**UT-C₁₁**: m = 10
**UT-C₁₂**: m = 11

**Figure 1.** Chemical structures of the UT monomers used in this study.

**Scheme 1.** Synthetic route towards (A) **UT-C$_{10}$**, **UT-C$_{11}$** and **UT-C$_{12}$** and (B) functionalized **UT-C$_{11}$-Cy3**. Reaction conditions: (a) THF, 44% (**1a**) 47% (**1b**) 98% (**1c**) (b) MeOH, Pd/C, H$_2$, 92% (**UT-C$_{10}$**) 72% (**UT-C$_{11}$**) 80% (**UT-C$_{12}$**) (c) THF, −70°C (1), TEA, 0°C (2), 15% (d) CuSO$_4$, NaAsc, Bim(Py)$_2$, aminoguanidine, DMF/H$_2$O, 88%.

To illustrate the use of 2,4-toluene-diisocyanate (TDI) as an accessible building block for desymmetrization, **UT-C$_{11}$-N$_3$** monomer was synthesized in a one pot reaction (Scheme 1B). Starting from TDI, first the azide terminated side chain was introduced by performing the amine-isocyanate reaction at −70°C. Since the isocyanate next to the methyl group is less reactive due to steric hindrance, this gave predominantly singly substituted product (~70%, urea formation on the 4 position, see Figure S1). Subsequent addition of the next amine with the alcohol terminated side chain at 0°C gave a mixture of compounds containing two, one or no azides. Normal phase chromatography was used to separate the fractions with two or no azides from the desired **UT-C$_{11}$-N$_3$**. However, LC-MS indicated the presence of the alkyl-hexa(ethylene glycol) side product, therefore reverse phase chromatography was used for additional purification. Although this reduced the yield to 15%, **UT-C$_{11}$-N$_3$** was hereby obtained without the side product. Since both the di-azide and diol side products are valuable, this is a promising approach to obtain desymmetrized building blocks based on TDI. In the final step, **UT-C$_{11}$-N$_3$** was reacted with alkyne functionalized Cy3 dye to obtain fluorescently labelled **UT-C$_{11}$-Cy3**. Attaching this fluorescent dye illustrates the potential of introducing functional groups by selectively reacting on only one of the side chains of the supramolecular monomer. All final products were characterized by $^1$H NMR, $^{13}$C NMR, matrix assisted laser desorption ionization-time-of-flight mass spectrometry (MALDI-TOF-MS), or liquid chromatography-mass spectrometry (LC-MS) (see the Supporting Information, Figures S2–S30).

## Self-assembly in water

After obtaining the supramolecular monomers, **UT-C$_{10}$**, **UT-C$_{11}$** and **UT-C$_{12}$** were assembled in water and the formed morphologies were visualized with cryo-TEM (Figures 2A–C, Figures S31–33). **UT-C$_{10}$** formed short fibrous assemblies, with many chain ends visible (Figure 2A). For **UT-C$_{11}$** long fibrous assemblies were visible, without any chain ends (Figure 2B). Long fibrous assemblies were also visible for **UT-C$_{12}$**, but some chain ends were observed as well (Figure 2C). The diameter of the fibers ranges from 7 to 9 nm. Interestingly, some periodicity in the images is observed, especially for **UT-C$_{11}$** and partly also for **UT-C$_{12}$**. A similar periodicity was observed previously for **BTA-(OH)$_3$** assemblies, where detailed cryo-TEM analysis revealed a double helix formation, possibly driven by additional hydrophobic shielding.[19,46] Since the **UT-C$_{11}$** and **UT-C$_{12}$** assemblies comprise two side chains instead of three, it is likely that the fibrous structures formed here also comprise more than 1 monomer in the cross section, as a consequence of hydrophobic shielding of the core.

To further investigate the nature of the formed fibrous structures, UV-Vis spectroscopy was utilized in combination with Fourier-transform infrared (FTIR) spectroscopy and Nile Red fluorescence experiments (Figure 2D–E).[19] The UV spectra of **UT** in aqueous solution are all similarly shaped, with a maximum at 211 nm, a shoulder at 246 nm and a small absorption at 286 nm (Figure 2D). The FTIR spectra in D$_2$O were also similar (Figure 2E) and we focus on the CO stretch vibration due to the overlap of N−D characteristic vibrations with D$_2$O.[47] The CO stretch is located at 1621 cm$^{-1}$ for all monomers (Figure 2E), indicating that all three **UT** monomers assemble with a similar hydrogen-bond pattern in water. Evidence that the **UT** monomers assemble into fibrous structures with hydro-
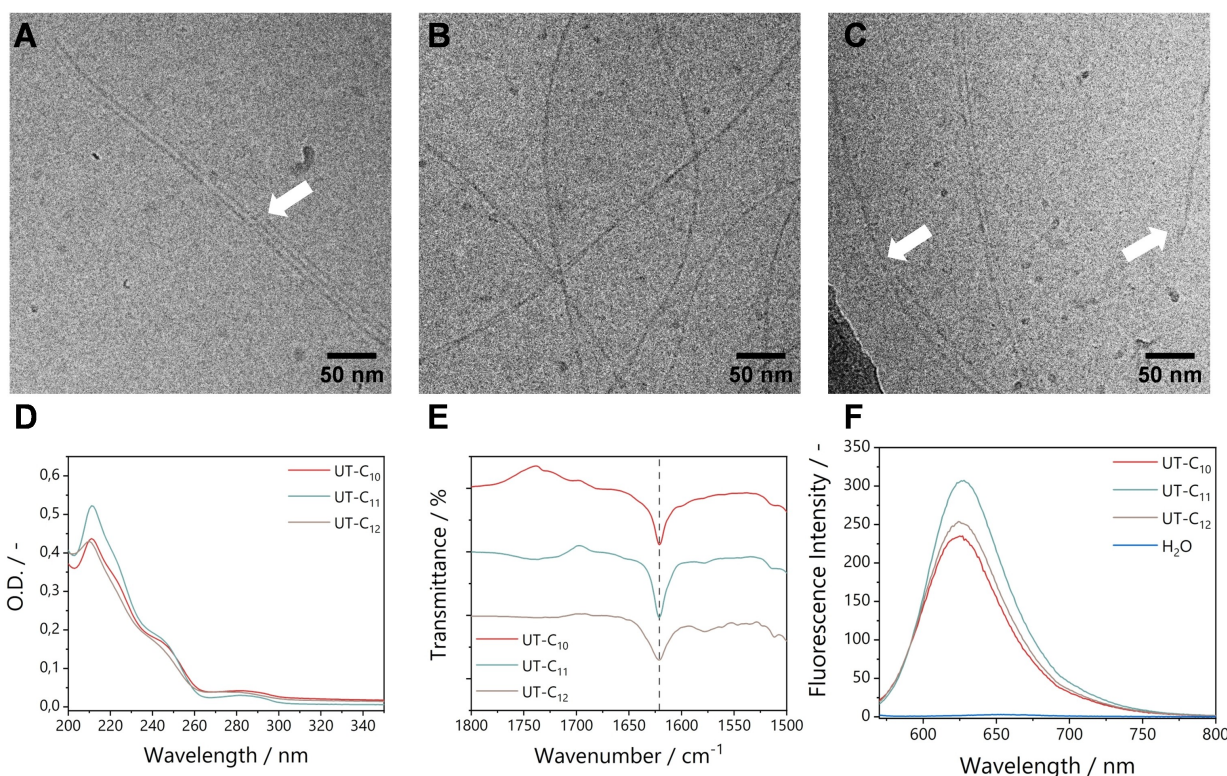
Chemistry–A European Journal

Research Article
doi.org/10.1002/chem.202303361

Chemistry
Europe
European Chemical
Societies Publishing

**Figure 2.** (A–C) Cryo-TEM images of (A) **UT-C$_{10}$** (B) **UT-C$_{11}$** and (C) **UT-C$_{12}$** assemblies in water ($c = 750$ μM). Chain ends are indicated with the white arrow. (D) UV-Vis of **UT-C$_{10}$**, **UT-C$_{11}$** and **UT-C$_{12}$** in water ($c = 250$ μM, $l = 1$ mm, $T = 20$ °C) (E) Zoom of the FTIR spectrum of the amide I vibration of **UT-C$_{10}$**, **UT-C$_{11}$** and **UT-C$_{12}$** in D$_2$O ($c = 20$ mg/mL, $l = 0.05$ mm, $T = 20$ °C). (F) Fluorescence emission spectra of Nile Red in solutions of **UT-C$_{10}$**, **UT-C$_{11}$**, **UT-C$_{12}$** and in water. ($c_{UT} = 250$ μM, $c_{NR} = 12.5$ μM, $l = 1$ mm, $T = 20$ °C).

phobic interiors was obtained by using the solvatochromic dye Nile Red (NR) as a probe. NR accumulates into hydrophobic domains where it becomes strongly fluorescent.[48] After formation of the solutions in water, 5 mol% NR was added and the solutions were equilibrated. Compared to pure water, the fluorescence intensity of NR increased and a large blue shift is observed for all assemblies (Figure 2F). The $\lambda_{max}$ for the three assemblies is similar (625 nm for **UT-C$_{10}$** and **UT-C$_{12}$** and 627 nm for **UT-C$_{11}$**), indicating the formation of hydrophobic interiors of similar polarities. A comparison can be made with the well-studied water-soluble **BTA-(OH)$_3$**, which forms supramolecular fibers in water with a $\lambda_{max}$ of 612 nm upon addition of NR.[29] The hydrophobic interior formed by the **UT** assemblies is more polar than those formed by **BTA-(OH)$_3$** assemblies. This could be due to less efficient shielding of the hydrophobic regions as **UT** monomers contain two side chains, while the **BTA-(OH)$_3$** monomers contain three.

To gain insight into the shape and size of the formed assemblies, small angle neutron scattering (SANS) experiments were carried out in D$_2$O (Figure 3, Figures S34–S36). Due to the high contrast between the deuterated solvent and the hexa(ethylene glycol)-based side chains, information can be extracted about the fully hydrated structure of the assemblies. The three scattering curves show a characteristic bump at high $q$ but have rather different power law at low $q$. A power law analysis at low $q$ revealed slopes of $-1.2$ for **UT-C$_{10}$** and $-1.1$ **UT-C$_{11}$**, indicative for the formation of long cylindrical structures
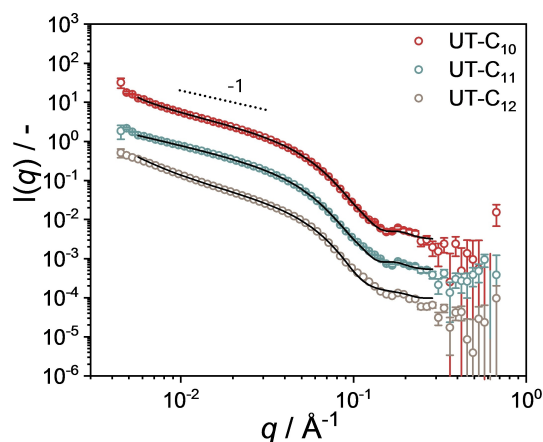


**Figure 3.** SANS scattering profiles (symbols) and corresponding elliptical cylinder fits (black line) in D$_2$O. Data is shifted vertically for clarity. ($c = 4.5$ mM).

in solution (Figure 3, S34). For **UT-C$_{12}$**, in contrast, a slope of $-1.5$ was found, suggesting that there are not solely cylindrical structures in solution. Previous work by the group of Bouteiller on a similar water-soluble bisurea system with an 11 carbon alkyl spacer showed that the scattering curves can be fit with an elliptical cylinder model.[40] Therefore, this model was also applied to assemblies formed by **UT** monomers (Figure 3, black lines).

**Chemistry–A European Journal**

Research Article
doi.org/10.1002/chem.202303361

**Chemistry Europe**
European Chemical
Societies Publishing

The parameters obtained from the fits are summarized in Table 1. Upon increasing the aliphatic chain length from 10 to 11 carbon atoms, an increase in the long cross-sectional diameter is visible, concurrent with a larger molecule size. Both short and long cross-sectional diameters are comparable to values obtained by the group of Bouteiller for a similar water-soluble bisurea system, indicating that there is more than 1 UT molecule in the cross-section.[40] The number of molecules in the cross-section lies between 3 and 5 (see Supporting Information for details). The values from the fit obtained for the **UT-C$_{11}$** monomer studied here are in accordance with a similar monomer with an 11 carbon alkyl spacer studied by the group of Bouteiller.[40] Here, the existence of multiple monomers in the cross-section was explained by lateral packing of the monomers due to solvophobic interactions in water. The long cross-sectional diameter of the cylinder of 10 nm matches the length of the **UT** monomers in a fully extended conformation,

including the hexa(ethylene glycol). Gratifyingly, the obtained values from the fits for the long cross-sectional diameter of the cylinder match the width of the assemblies visualized with cryo-TEM. We propose a schematic representation of the assemblies as shown in Figure 4.

Thus, cryo-TEM revealed that all **UT** monomers form elongated structures in solution, with differences in the length of the assemblies. UV-Vis, FTIR, fluorescence spectroscopy, and SANS indicate the formation of assemblies in water of similar nature and with similar packing, regardless of length of alkyl spacer. To investigate if the length of the alkyl spacer has an effect on the stability of the formed assemblies, temperature dependent UV-Vis spectroscopy was carried out. Heating the solutions to 90 °C revealed the differences in stability between the three assemblies. Assemblies formed by **UT-C$_{10}$** are stable up to 50 °C (Figure 5A). At temperatures above 50 °C, the intensity at 211 nm decreases, concurrent with an increase of the absorption bands at 225 and 248 nm, indicating a loss of hydrogen bonding and different type of packing at elevated temperatures. Assemblies formed by **UT-C$_{11}$** (Figure 5B) do not show this shift in absorption upon heating, but instead show a gradual increase of scattering, indicating phase separation in the solution, which may result from LCST behavior of the molecule. Finally, assemblies formed by **UT-C$_{12}$** (Figure 5C) do not show any transitions up to 90 °C. Increasing the alkyl spacer length thus increases the stability of the assemblies.

**Table 1.** Parameters obtained from SANS fits as shown in Figure 4. 2xa is the short cross-sectional diameter of the ellipse, and 2xb is the long cross-sectional diameter of the ellipse. L is the length of the cylinders. n is the number of molecules in the cross-section, assuming a repeat distance of 4.6 Å.[32] Details on fitting can be found in the Supporting Information.

| Monomer | 2xa [Å] | 2xb [Å] | L [Å] |
|---|---|---|---|
| UT–C10 | 50 ± 0 | 93 ± 0 | ≥ 2000 |
| UT–C11 | 52 ± 0 | 100 ± 0 | ≥ 2000 |
| UT–C12 | 52 ± 0 | 88 ± 0 | ≥ 2000 |



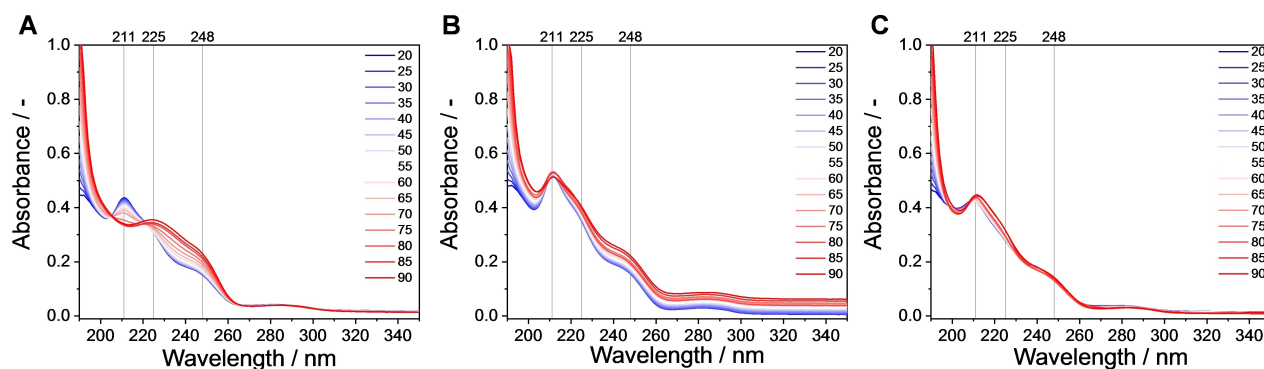**Figure 4.** (A) Schematic representation of the structures formed by the **UT** monomers in water.

### Dynamic exchange of UT monomers

From the above results, it becomes clear that **UT** monomers form fibrous structures in water, with increased core radius and thermal stability upon increasing the hydrophobic alkyl spacer. To investigate the dynamic behavior of the structures, and to compare monomer dynamics between the structures, hydrogen deuterium exchange followed by mass spectrometry (HDX-MS) was employed. HDX-MS is a label free method previously used in our group to investigate exchange processes in supramolecular polymers.[20,21,49] Hereto, assemblies were diluted 100× in D$_2$O; this high dilution did not affect the nature of the assemblies as evidenced by UV spectra (Figure S36). The exchange of labile hydrogen atoms into deuterium was



**Figure 5.** Temperature-dependent UV-Vis spectroscopy for (A) **UT-C$_{10}$** (B) **UT-C$_{11}$** and (C) **UT-C$_{12}$** assemblies in water (c = 25 μM, l = 10 mm).

followed over time with MS (Figure 6, Supporting Information for details on calculations of the percentages of deuterated species).

The monomers used in this work have six exchangeable hydrogen atoms, of which two are peripheral OH atoms located on the outside of the assembly, and four bisurea NHs which are located in the hydrophobic regions. The two OHs immediately exchange due to direct contact with $D_2O$, but the exchange of the bisurea NHs is slowed down and can thus give insights into the dynamicity and degree of order of the system either by exchange of a monomer between different assemblies, or by penetration of $D_2O$ into the fibrous structure. Exchange due to monomer release into the surrounding $D_2O$ is expected to give rise to UT6D species, whereas $D_2O$ penetration within less ordered regions of the supramolecular polymers gives rise to intermediate UT-3D, -4D and -5D species.[20]

To compare the monomer exchange dynamics, the percentage of fully deuterated species (UT6D) is plotted in Figure 6A. For all systems, a fast initial increase of UT6D is visible, which levels off after 1 to 4 h, depending on alkyl chain length. With increasing alkyl chain length, the percentage of UT6D decreases, indicating more ordered and stable assemblies, corroborating the results obtained with temperature-dependent UV-Vis. In addition, more pronounced differences are visible in the first few hours (Figure 6B–D). The intermediate species are plotted here as well to gain more insight into the H/D exchange. For **UT-C$_{10}$** (Figure 6B), after three minutes, already 80% of the molecules is fully deuterated. For **UT-C$_{11}$** (Figure 6C),

the initial exchange leads to 38% fully deuterated species and for **UT-C$_{12}$** (Figure 6D) only 4% fully deuterated species is observed. The fast initial exchange to fully deuterated species could be due to defects within the assembly which lead to a combination of rapid solvent penetration and rapid release of monomers into the environment, but the presence of these defects decreases upon increasing length of alkyl chain length. In addition, the transition point from initially fast H/D exchange to slow H/D exchange shifts upon increasing the alkyl chain length. For **UT-C$_{10}$** this transition occurs after 10 min, for **UT-C$_{11}$** around 1 h and for **UT-C$_{12}$** after 4 h. These timescales overlap with timescales where solvent penetration is observed, suggesting that the early H/D exchange arises from less-ordered regions in the assemblies. The longer the hydrophobic alkyl chains, the longer it takes for these regions to exchange. After this transition point, the exchange is governed by monomer release from the assemblies. For **UT-C$_{11}$** and **UT-C$_{12}$** systems, complete H/D exchange is never observed, suggesting that some regions in the fiber's interior are inaccessible or highly organized. A similar phenomenon was observed for previously studied BTAs and an aliphatic bisurea system, but the exact reason for this behavior is still ill-understood.[21]

Interestingly, all the observations regarding H/D exchange are comparable to what was observed for **BTA-(OH)$_3$** based assemblies with varying alkyl chain lengths.[20] This makes the **UT** system an interesting platform for more accessible desymmetrization and functionalization.
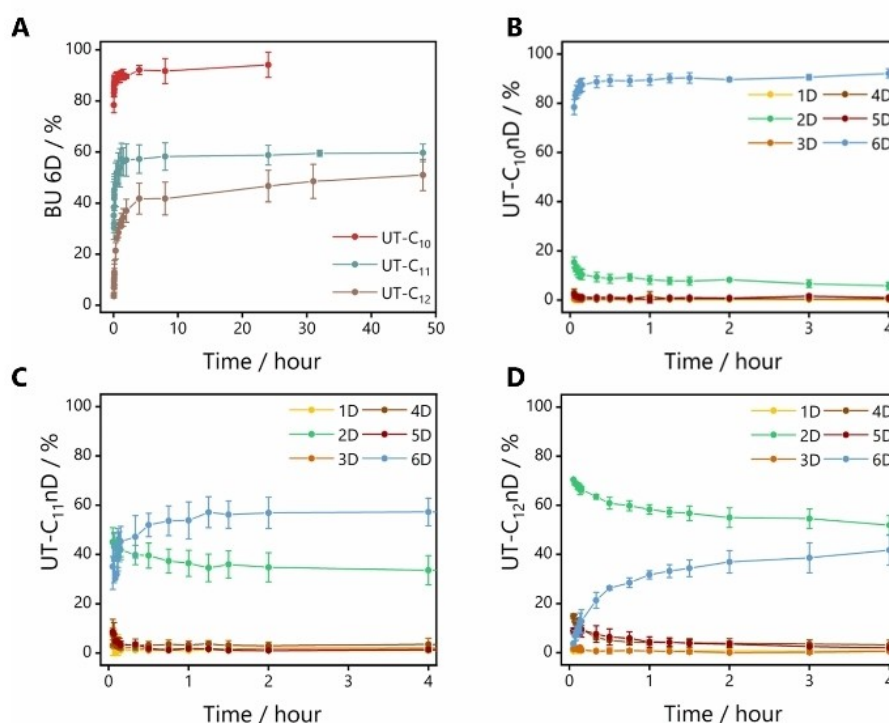


**Figure 6.** (A) Percentage of fully deuterated species (BU 6D) for all three **UT** monomers over time. (B–D) The percentage of different deuterated analogues of (B) **UT-C$_{10}$** (C) **UT-C$_{11}$** (D) **UT-C$_{12}$** as a function of time after the 100x dilution of an aqueous sample into $D_2O$ with 0.5 M NaAc (T = room temperature). The symbols represent the average and the error bars the standard deviation calculated from three independent measurements. The lines are added as a guide to the eye. ($c_{initial}$ = 1 mM, $c_{diluted}$ = 10 μM).

**Chemistry–A European Journal**

Research Article
**doi.org/10.1002/chem.202303361**

**Chemistry Europe**
European Chemical
Societies Publishing

## Exploration of UTs as biomaterial

To assess the potential as biomaterial, **UT-C$_{11}$** was chosen for further investigation as these assemblies seemed most promising based on their dynamic behavior, stability and long fibrous morphology. First, we investigated whether the assemblies affected the metabolic activity of cells using two different cell types. Hereto, the **UT-C$_{11}$** assemblies were incubated with two different cell types (HeLa and human normal dermal fibroblasts (hNDFs) (Figure 7A, B). HeLa cells are epithelial cells and a robust and commonly used diseased human cell line. hNDFs are fibroblasts with were selected as healthy cell line. The **UT-C$_{11}$** fibers were incubated with the different cell types with increasing concentrations of **UT-C$_{11}$** for 24 h. The metabolic activity of the cells was assessed using a resazurin viability assay, where viable cells convert non-fluorescent resazurin into fluorescent resorufin. Gratifyingly, the **UT-C$_{11}$** fibers did not affect the metabolic activity of the cells up to 250 µM concentrations for both cell types. This suggests that the fibers do not exhibit toxic effects to the cells, making the **UT** platform a good candidate for biomaterial development.

To investigate the stability of the assemblies in conditions used for biological experiments (low concentration, biological media), **UT-C$_{11}$** was co-assembled with 5% **UT-C$_{11}$-Cy3**. Because only a fraction of monomers typically needs to be functionalized for biomedical applications, we selected 5% for initial tests. First, the incorporation of the dye labeled **UT-C$_{11}$-Cy3** and the morphology at low concentrations in water was assessed with

total internal reflection fluorescence microscope (TIRF) microscopy (Figure 7C), where micrometer long fibers were visible. Thus, **UT-C$_{11}$-Cy3** is incorporated into the assemblies (5% incorporation) and at low concentration (2.5 µM total concentration) the co-assemblies remain stable. Then, the behavior of the assemblies in presence of fetal bovine serum (FBS) was assessed, as FBS is typically used in cell culture media. Hereto, **UT-C$_{11}$** fibers were incubated overnight at 37 °C in PBS with 10% FBS. Compared to the assemblies in water, the fibers were shorter but still clearly present (Figure 7D) indicating that FBS is capable of interacting with the assemblies, but not to completely degrade them. The shortening of assemblies by interaction with proteins has also been observed for **BTA** based supramolecular polymers, and was ascribed to interaction with hydrophobic patches present on the proteins.[50] To further mimic the complex environment used for cell culturing, the **UT-C$_{11}$** fibers were incubated overnight at 37 °C in DMEM cell medium containing 10% FBS. Again, short and long assemblies were visible, showing that the assemblies were shortened due to interaction with the protein, but also that the fiber morphology is retained (Figure 7E).

The results presented above clearly indicate that UT fibers are not only compatible with cells, but also retain a fiber morphology in cell culture media. This last observation is of high importance as it implies that UT-based fibers form very stable morphologies. The latter is a crucial factor for systems to be used as biomaterials.
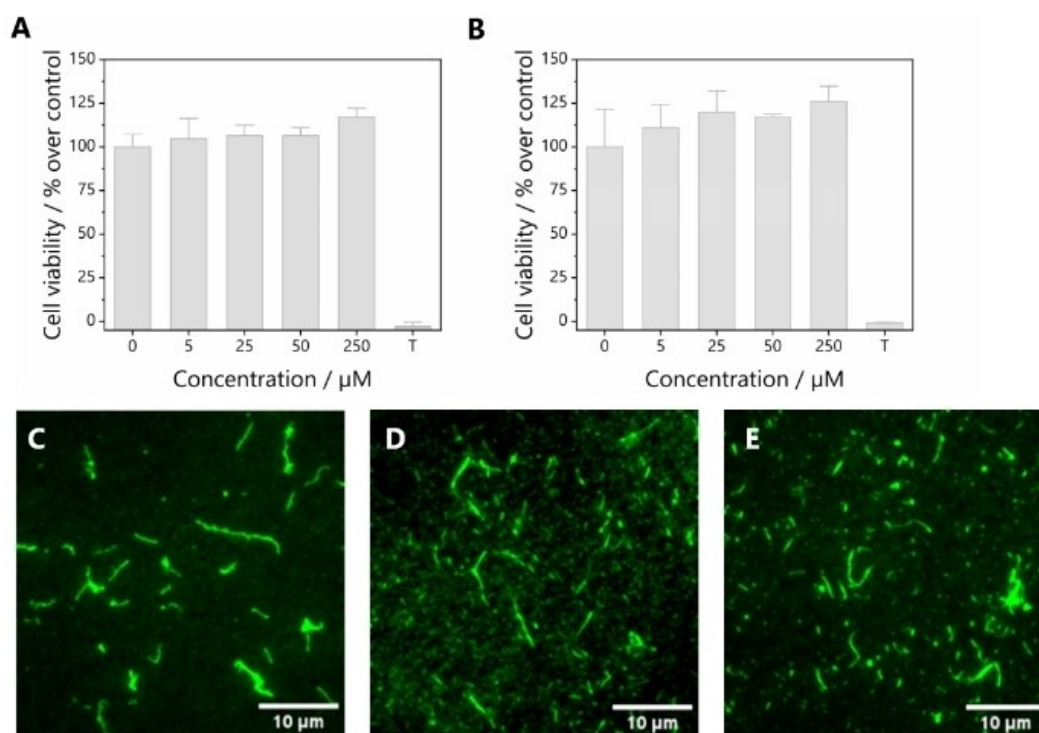


**Figure 7.** Suitability of UT as biomaterial (A–B) Cell viability for (A) HeLa cells and (B) hNDFs was determined with a resazurin assay. The material was exposed to hNDFs and HeLa cells in complete culture medium. The cell viability is normalized on corresponding cells that were cultured in untreated medium (i.e. 0 µM concentration). Cells treated with Triton X-100 were used as negative control (T). A concentration of 250 µM corresponds to 0.269 mg/mL **UT-C$_{11}$**. (C–E) TIRF images of **UT-C$_{11}$** fibers labeled with 5% **UT-C$_{11}$-Cy3** upon overnight incubation in (C) MQ water at room temperature. (D) PBS buffer with 10% FBS at 37 °C. (E) DMEM medium with 10% FBS at 37 °C. (c$_{total}$ = 2.5 µM, UT-C$_{11}$-Cy3 5%, with respect to total UT concentration).

**Chemistry–A European Journal**

Research Article
doi.org/10.1002/chem.202303361

**Chemistry**
**Europe**
European Chemical
Societies Publishing

## Conclusions

In summary, the **UT** motif was used for preparing water-compatible supramolecular polymers with the aim to explore their potential as biomaterials. Starting from toluene-2,4-diisocyanate, three **UT** monomers were synthesized with a variation in alkyl chain length by reaction with their respective amine-modified side chains (**UT-C$_{10}$, UT-C$_{11}$** and **UT-C$_{12}$**). All three monomers were capable of forming elongated assemblies in water driven by hydrogen bonding, with the formation of hydrophobic regions. Subtle differences were found upon assembly in water by visualizing the structures with cryo-TEM, where **UT-C$_{11}$** formed homogeneous long assemblies, while **UT-C$_{10}$** and **UT-C$_{12}$** showed the formation of shorter structures. The variation of the alkyl chain length mainly influenced the stability and dynamicity of the supramolecular assemblies; an increase of the alkyl chain length lead to an increased thermal stability and decreased dynamics, as probed by HDX-MS. In addition, the **UT** motif was readily obtained in desymmetrized form by replacing one OH group for an azide group in a one-pot reaction. Conjugation of a dye label allowed for visualization of the copolymers, and highlighted the ability to introduce function in the future. The results showed that the **UT-C$_{11}$** assemblies retain their morphology upon copolymerization and that the fibrous morphology is retained even at the low concentrations typically used for biological assays. Finally, the stability in complex media and the absence of toxic effects on two cell lines opens up possibilities to use the **UT** motif to access water-compatible supramolecular polymers as biomaterials. This will be the topic of future investigations.

## Experimental Section

**Assembly of UT materials**. *Self-assembly:* Solid materials were weighed and dissolved in MeOH to create a stock solution. From this stock solution, the desired amount was taken and the organic solvent was removed using an N$_2$ (g) stream after which MQ water was added to obtain the desired concentration. After vortexing to solubilize the formed film inside the vial, the sample was stirred at 80 °C for 15 min and vortexed for 15 s immediately afterwards. All samples were left to equilibrate overnight at room temperature before being used for the measurements. *Co-assembly with dye labeled UT.* The similar procedure was followed as for the assembly, but with an additional step of adding **UT-C$_{11}$-Cy3** from a stock solution in MeOH (500 μM) after vortexing. The samples were then equilibrated at 45 °C for 15 min without stirring. The samples were left to equilibrate overnight at room temperature and were further equilibrated in the refrigerator for one week until the measurements to prevent degradation of the dye.

**Cell viability assay**. A resazurin assay was used to assess whether the materials affect the metabolic activity of the cells. To this end, human normal dermal fibroblasts (hNDFs) or HeLa cells were seeded at a density of $5 \times 10^3$ or $10 \times 10^3$ cells, respectively, per well in a 96-well plate containing 100 μL complete culture medium. hNDF were cultured in DMEM advanced medium (Gibco) supplemented with 10 v/v% fetal bovine serum (FBS), 1 v/v% penicillin streptomycin (P/S) and 1 v/v% Gluta MAX. HeLa cells were cultured in DMEM (Gibco) containing 0.11 g/L sodium pyruvate, 2 mM L-glutamine and 4.5 g/L glucose and further supplemented with 10 v/v% FBS and 1 v/v% P/S. Cells were incubated at 37 °C and 5%

CO$_2$ and maintained under standard culturing conditions until grown to 70% confluence. Next, the cells were cultured in the presence of the UV-sterilized materials in 100 μL fresh culture medium for an additional 24 h. The assemblies were diluted from a stock concentration of 2.5 mM to obtain the target concentration. The next day, cell viability was assessed by adding 44 μM resazurin in fresh culture medium to the cells. The cells were incubated under standard culturing conditions for 3 h. Viable cells convert non-fluorescent resazurin into fluorescent resorufin ($\lambda_{ex}=530$ nm, $\lambda_{em}=590$ nm), which was measured on a Synergy HT plate reader in 90 μL in triplicate per well in a black 96-well plate. Each condition was tested 4 times, except for the 50 μM condition which was tested 2 times. Background subtraction (wells with only medium, without cells) was performed for all measurements. Cell viability in percentage is presented relative to the viability of hNDFs or HeLa cells that were cultured in untreated cell medium during the course of the experiment. This value was set at 100% cell viability. Cells treated with Triton X-100 were used as negative control.

**Synthesis of UT-C10**. 1,1′-(4-Methyl-1,3-phenylene)bis(3-(1-phenyl-2,5,8,11,14,17,20-heptaoxatriacontan-30-yl)urea) (1a) (146.7 mg, 119.4 μmol, 1 equiv.) was dissolved in MeOH in a 3-neck round bottom flask. The mixture was bubbled through with N$_2$-gas for 20 min. At room temperature and with the addition of the Pd/C catalyst (10 wt.%, 1 equiv.), the mixture was stirred under H$_2$ gas overnight. The mixture was then glass filtered over celite and washed twice with 60 mL MeOH. The resulting solution was concentrated in vacuo to obtain the final product **UT-C10** as a sticky solid (115.7 mg, 109.2 μmol, 92%). $^1$H NMR (400 MHz, DMSO-$d6$): δ 8.24 (s, 1H, Ar-NH), 7.71 (d, $J=2.2$ Hz, 1H, Ar–H), 7.47 (s, 1H, Ar-NH), 7.11 (dd, $J=8.2, 2.2$ Hz, 1H, Ar–H), 6.91 (d, $J=8.3$ Hz, 1H, Ar–H), 6.49 (t, $J=5.5$ Hz, 1H, CH$_2$-NH), 5.94 (t, $J=5.7$ Hz, 1H, CH$_2$-NH), 4.56 (t, $J=5.5$ Hz, 2H, CH2CH2-OH), 3.53–3.43 (m, 44H, O-(CH$_2$)$_2$O), 3.41 (t, $J=5.0$ Hz, 4H, CH$_2$CH$_2$CH$_2$O), 3.35 (t, $J=6.6$ Hz, 4H, CH$_2$CH$_2$-OH), 3.05 (dq, $J=12.5, 6.5$ Hz, 4H, CH$_2$CH$_2$-NH), 2.07 (s, 3H, Ar-CH$_3$), 1.52–1.37 (m, 8H, aliphatic), 1.25 (d, $J=4.1$ Hz, 24H, aliphatic). $^{13}$C NMR (100 MHz, DMSO-$d6$): δ 155.79, 155.74, 139.17, 138.72, 130.29, 79.66, 72.82, 70.78, 70.29, 70.26, 70.24, 69.94, 60.67, 40.62, 40.42, 40.21, 40.00, 39.79, 39.58, 39.43, 39.37, 30.30, 30.22, 29.68, 29.49, 29.36, 29.29, 26.93, 26.88, 26.13, 17.70. MALDI-ToF: Chemical formula: C$_{53}$H$_{100}$N$_4$O$_{16}$. Calculated m/z: 1048.71 g/mol. Measured m/z: 1071.67 [M+Na]+, 1087.66 [M+K]+.

**Synthesis of UT-C11**. The same same procedure as described for **UT-C10**, but starting with 1,1′-(4-methyl-1,3-phenylene)bis(3-(1-phenyl-2,5,8,11,14,17,20-heptaoxahentriacontan-31-yl)urea) (1 b) (146.3 mg, 116 μmol, 1 equiv.). The final product **UT-C11** was obtained as a sticky solid (92.9 mg, 85.39 μmol, 72%). $^1$H NMR (400 MHz, DMSO-$d6$): δ 8.32 (s, 1H, Ar-NH), 7.70 (d, $J=2.2$ Hz, 1H, Ar–H), 7.52 (s, 1H, Ar-NH), 7.12-7.10 (dd, $J=8.2, 2.2$ Hz, 1H, Ar–H), 6.92-6.90 (d, $J=8.3$ Hz, 1H, Ar–H), 6.54 (t, $J=5.5$ Hz, 1H, CH$_2$-NH), 6.05 (t, $J=5.7$ Hz, 1H, CH$_2$-NH), 4.58 (t, $J=5.5$ Hz, 2H, CH$_2$CH$_2$-OH), 3.51-3.40 (m, 44H, O-(CH$_2$)$_2$-O), 3.41 (t, $J=5.0$ Hz, 4H, CH$_2$CH$_2$CH$_2$O), 3.35 (t, $J=6.6$ Hz, 4H, CH$_2$CH$_2$-OH), 3.05 (dq, $J=12.5, 6.5$ Hz, 4H, CH$_2$CH$_2$-NH), 2.07 (s, 3H, Ar-CH$_3$), 1.48-1.30 (m, 8H, aliphatic), 1.25 (d, $J=4.1$ Hz, 28H, aliphatic). 13 C NMR (100 MHz, DMSO-$d6$): δ 155.77, 155.72, 139.14, 138.72, 130.31, 79.66, 72.82, 70.78, 70.29, 70.26, 70.24, 69.95, 60.68, 40.62, 40.41, 40.20, 39.99, 39.79, 39.58, 39.50, 39.37, 30.30, 30.22, 29.68, 29.52, 29.47, 29.36, 29.29, 26.93, 26.87, 26.13, 17.70. MALDI-ToF: Chemical formula: C$_{55}$H$_{104}$N$_4$O$_{16}$. Calculated m/z: 1076.74. Measured m/z: 1099.76 [M+Na]+, 1115.73 [M+K]+.

**Synthesis of UT-C12**. The synthesis of **UT-C12** was performed following the same procedure as described for **UT-C10**, but starting with 1,1′-(4-methyl-1,3-phenylene)bis(3-(1-phenyl-2,5,8,11,14,17,20-heptaoxadotriacontan-32-yl)urea) (1 c) (899 mg, 1 equiv.) and after addition of Pd/C catalyst (10 wt.%, 4.42 equiv., 330 mg), the mixture was stirred under H$_2$ gas for four days. The final product **UT-C12**

**Chemistry–A European Journal**

Research Article
doi.org/10.1002/chem.202303361

**Chemistry Europe**
European Chemical
Societies Publishing

was obtained as a white solid (619 mg, 0.56 mmol, 80%). $^1$H NMR (400 MHz, DMSO-$d6$) δ 8.24 (s, 1H, Ar-NH), 7.71 (d, J = 2.2 Hz, 1H, Ar–H), 7.47 (s, 1H, Ar-NH), 7.11 (dd, J = 8.2, 2.2 Hz, 1H, Ar–H), 6.91 (d, J = 8.3 Hz, 1H, Ar–H), 6.49 (t, J = 5.5 Hz, 1H, CH$_2$-NH), 5.94 (t, J = 5.7 Hz, 1H, CH$_2$-NH), 4.56 (t, J = 5.5 Hz, 2H, CH$_2$CH$_2$-OH), 3.53 - 3.43 (m, 44H, O-(CH$_2$)$_2$-O), 3.41 (t, J = 5.0 Hz, 4H, CH$_2$CH$_2$CH$_2$O), 3.35 (t, J = 6.6 Hz, 4H, CH$_2$CH$_2$-OH), 3.05 (dq, J = 12.5, 6.5 Hz, 4H, CH$_2$CH$_2$-NH), 2.07 (s, 3H, Ar-CH$_3$), 1.52 - 1.37 (m, 8H, aliphatic), 1.25 (d, J = 4.1 Hz, 32H, aliphatic). $^{13}$C NMR (100 MHz, DMSO-$d6$) δ 155.71 (d, J = 7.2 Hz), 138.91 (d, J = 37.4 Hz), 130.33, 72.82, 70.78, 70.29, 70.26, 69.95, 60.68, 30.29, 30.21, 29.68, 29.53, 29.49, 29.36, 29.30, 26.92, 26.86, 26.13. MALDI-ToF: Calculated m/z = 1104.67, observed m/z = 1127.78 [M + Na] + . FTIR (ATR) ν (cm$^{-1}$): FTIR (ATR) ν (cm$^{-1}$): 3318, 2919, 2850, 1629, 1578, 1508, 1467, 1453, 1396, 1346, 1328, 1280, 1239, 1107, 999, 963, 879, 846, 812, 764, 720, 628, 591, 529.

**Synthesis of UT-C$_{11}$-N$_3$.** TDI (36.5 mg, 0.21 mmol, 1 equiv.) was dissolved in 10 mL dry THF in a 25 mL flask and cooled on a dry ice/acetone bath to −70 °C. 1-Azido-20-octyl-3,6,9,12,15,18-hexaoxahenicosan-21-amine (100 mg, 21 mmol, 1 equiv.) was dissolved in 1 mL THF and added dropwise over a period of 15 min. After one hour, NMR indicated that not all starting material had been consumed, so an additional amount of the amine (20 mg, 0.0425 mmol, 0.2 equiv.) was dissolved in 1 mL THF and slowly added dropwise. TEA (50 μL, 0.359 mmol, 1.7 equiv.) was added to the reaction mixture, after which 1-hydroxy-3,6,9,12,15,18-hexaoxanonacosan-29-aminium chloride (71 mg, 0.157 mmol, 0.75 equiv.) was dissolved in 1 mL THF and added. The reaction mixture was then allowed to warm up to 0 °C. After 1 h, NMR indicated no full conversion, thus an additional amount of the second amine (25 mg, 0.055 mmol, 0.26 equiv.) and 20 μL TEA in 1 mL CHCl$_3$ were added and the reaction mixture stirred for an additional hour. Then, the reaction mixture was transferred to a separation funnel and an additional 25 mL of CHCl$_3$ was added. The organic layer was washed twice with 10 mL water, once with 10 mL brine and the organic layer was dried with Na$_2$SO$_4$. The crude mixture was then purified with column chromatography (24 g SiO$_2$, MeOH/CHCl$_3$ 6/94). LCMS and TLC indicated the presence of the surfactant-like impurity, so the compound was further purified with reverse phase column chromatography (Sfaer 12 g, C18 silica gel, 20/80 to 100/0 ACN/H$_2$O). Lyophilization gave product UT-C$_{11}$-N$_3$ as a sticky white solid (35 mg, 0.032 mmol, 15% yield). $^1$H NMR (400 MHz, CDCl$_3$) δ 7.23 (s, 1H, Ar–H), 6.82 (d, J = 8.2 Hz, 1H, Ar–H), 6.67 (d, J = 10.7 Hz, 1H, Ar–H), 5.68 (s, 2H, CH$_2$-NH–), 3.78 - 3.51 (m, 44H, O-(CH$_2$)$_2$-O), 3.50 - 3.35 (m, 6H, CH$_2$CH$_2$-OH, CH$_2$CH$_2$CH$_2$O), 3.16 (q, J = 6.7 Hz, 4H, NH-CH$_2$-CH$_2$), 2.99 (s, 2H, CH$_2$-CH$_2$-N$_3$), 1.92 (s, 3H, Ar-CH$_3$), 1.64 - 0.99 (m, 36H, aliphatic). LCMS: Chemical formula: C$_{55}$H$_{103}$ N$_7$O$_{15}$. Calculated m/z: 1101.75. Measured m/z: 1124.75 [M + Na]$^+$, 563.00 [M + Na + H]$^{2+}$ (RT: 5.24 min).

**Synthesis of UT-C$_{11}$-Cy3.** UT-C$_{11}$-N$_3$ (7.467 mg, 0.067 mmol, 1 equiv.) was weighed off in an LCMS vial and dissolved in 500 μL DMF. Cy3-alkyne (5 mg, 0.10 mmol, 1.5 equiv.) was dissolved in 200 μL DMF and added. A separate click cocktail was prepared composed of 50 μL CuSO$_4$ (50 mM in H$_2$O), 50 μL BimPy2 (30 mM in DMF), 50 μL aminoguanidine (200 mM in H$_2$O) and freshly prepared sodium ascorbate (200 mM in H$_2$O). The click cocktail was gently shaken and added to the reaction mixture, which turned brown. The reaction mixture was slowly stirred at room temperature for 3 h, after which LC-MS showed full conversion. The crude reaction mixture was purified by a reverse phase column chromatography (12 g, C18 silica gel, 20/80 to 100/0 ACN/H$_2$O with 0.1% FA). After lyophilization the product UT-C$_{11}$-Cy3 was obtained as a sticky pink solid (9.5 mg, 0.06 mmol, 88%). LC-MS: Chemical formula: C$_{88}$H$_{143}$N$_{10}$O$_{16}$$^+$. Calculated m/z = 1597.07, observed m/z = 798.58 [M + H]$^{2+}$, 533 [M + 2H]$^{3+}$ (RT: 4.57 min).

## Supporting Information

Additional supplementary Information is available free of charge, comprising detailed synthetic procedures, full characterization of all products, additional fits of the SANS data and HDX-MS calculations. The authors have added references within the Supporting Information.[51–55]

## Conflict of Interests

The authors declare no conflict of interest.

## Data Availability Statement

The data that support the findings of this study are available in the supplementary material of this article.

[1] J. K. Mouw, G. Ou, V. M. Weaver, *Nat. Rev. Mol. Cell Biol.* **2014**, 15, 771–785.
[2] R. D. Vale, *Cell* **2003**, 112, 467–480.
[3] F. Van den Ent, L. A. Amos, J. Löwe, *Nature* **2001**, 413, 39–44.
[4] L. Brunsveld, B. J. B. Folmer, E. W. Meijer, R. P. Sijbesma, *Chem. Rev.* **2001**, 101, 4071–4098.
[5] T. Aida, E. W. Meijer, S. I. Stupp, *Science* **2012**, 335, 813–817.
[6] J. Boekhoven, S. I. Stupp, *Adv. Mater.* **2014**, 26, 1642–1659.
[7] N. M. Casellas, L. Albertazzi, S. Pujals, T. Torres, M. García-Iglesias, *Chem. Eur. J.* **2021**, 27, 11056–11060.
[8] N. M. Casellas, S. Pujals, D. Bochicchio, G. M. Pavan, T. Torres, L. Albertazzi, M. García-Iglesias, *Chem. Commun.* **2018**, 54, 4112–4115.
[9] P. Besenius, *J. Polym. Sci. Part A* **2017**, 55, 34–78.
[10] E. Krieg, M. M. C. Bastings, P. Besenius, B. Rybtchinski, *Chem. Rev.* **2016**, 116, 2414–2477.
[11] M. J. Webber, E. A. Appel, E. W. Meijer, R. Langer, *Nat. Mater.* **2015**, 15, 13–26.
[12] A. Mata, Y. Geng, K. J. Henrikson, C. Aparicio, S. R. Stock, R. L. Satcher, S. I. Stupp, *Biomaterials* **2010**, 31, 6004–6012.

**Chemistry–A European Journal**

Research Article
doi.org/10.1002/chem.202303361

Chemistry
Europe

European Chemical
Societies Publishing

[13] S. S. Lee, T. Fyrner, F. Chen, Z. Álvarez, E. Sleep, D. S. Chun, J. A. Weiner, R. W. Cook, R. D. Freshman, M. S. Schallmo, K. M. Katchko, A. D. Schneider, J. T. Smith, C. Yun, G. Singh, S. Z. Hashmi, M. T. McClendon, Z. Yu, S. R. Stock, W. K. Hsu, E. L. Hsu, S. I. Stupp, *Nat. Nanotechnol.* **2017**, *12*, 821–829.

[14] Z. Álvarez, A. N. Kolberg-Edelbrock, I. R. Sasselli, J. A. Ortega, R. Qiu, Z. Syrgiannis, P. A. Mirau, F. Chen, S. M. Chin, S. Weigand, E. Kiskinis, S. I. Stupp, *Science* **2021**, *374*, 848–856.

[15] S. I. S. Hendrikse, S. P. W. Wijnands, R. P. M. Lafleur, M. J. Pouderoijen, H. M. Janssen, P. Y. W. Dankers, E. W. Meijer, *Chem. Commun.* **2017**, *53*, 2279–2282.

[16] M. H. Bakker, R. E. Kieltyka, L. Albertazzi, P. Y. W. Dankers, *RSC Adv.* **2016**, *6*, 110600–110603.

[17] M. Diba, S. Spaans, S. I. S. Hendrikse, M. M. C. Bastings, M. J. G. Schotman, J. F. van Sprang, D. J. Wu, F. J. M. Hoeben, H. M. Janssen, P. Y. W. Dankers, *Adv. Mater.* **2021**, *33*, 2008111.

[18] J. Song, M. G. J. Schmitz, M. Riool, S. Guo, S. A. J. Zaat, P. Y. W. Dankers, *J. Polym. Sci.* **2023**, *61*, 2866–2877.

[19] C. M. A. Leenders, L. Albertazzi, T. Mes, M. M. E. Koenigs, A. R. A. Palmans, E. W. Meijer, *Chem. Commun.* **2013**, *49*, 1963–1965.

[20] X. Lou, R. P. M. Lafleur, C. M. A. Leenders, S. M. C. Schoenmakers, N. M. Matsumoto, M. B. Baker, J. L. J. Van Dongen, A. R. A. Palmans, E. W. Meijer, *Nat. Commun.* **2017**, *8*, 1–8.

[21] X. Lou, S. M. C. Schoenmakers, J. L. J. van Dongen, M. Garcia-Iglesias, N. M. Casellas, M. Fernández-Castaño Romera, R. P. Sijbesma, E. W. Meijer, A. R. A. Palmans, *J. Polym. Sci.* **2021**, *59*, 1151–1161.

[22] P. Ahlers, H. Frisch, P. Besenius, *Polym. Chem.* **2015**, *6*, 7245–7250.

[23] H. Frisch, Y. Nie, S. Raunser, P. Besenius, *Chem. Eur. J.* **2015**, *21*, 3304–3309.

[24] M. Von Gröning, I. De Feijter, M. C. A. Stuart, I. K. Voets, P. Besenius, *J. Mater. Chem. B* **2013**, *1*, 2008–2012.

[25] E. Fuentes, Y. Gabaldón, M. Collado, S. Dhiman, J. A. Berrocal, S. Pujals, L. Albertazzi, *J. Am. Chem. Soc.* **2022**, *144*, 21196–21205.

[26] E. Fuentes, M. Gerth, J. A. Berrocal, C. Matera, P. Gorostiza, I. K. Voets, S. Pujals, L. Albertazzi, *J. Am. Chem. Soc.* **2020**, *142*, 10069–10078.

[27] D. Straßburger, N. Stergiou, M. Urschbach, H. Yurugi, D. Spitzer, D. Schollmeyer, E. Schmitt, P. Besenius, *ChemBioChem* **2018**, *19*, 912–916.

[28] G. Morgese, B. F. M. Waal, S. Varela-Aramburu, A. R. A. Palmans, L. Albertazzi, E. W. Meijer, *Angew. Chem. Int. Ed.* **2020**, *132*, 17382–17386.

[29] S. M. C. Schoenmakers, B. W. L. van den Bersselaar, S. Dhiman, L. Su, A. R. A. Palmans, *Org. Biomol. Chem.* **2021**, *19*, 8281–8294.

[30] T. Klein, F. V. Gruschwitz, S. Rogers, S. Hoeppener, I. Nischang, J. C. Brendel, *J. Colloid Interface Sci.* **2019**, *557*, 488–497.

[31] F. V. Gruschwitz, M. C. Fu, T. Klein, R. Takahashi, T. Higashihara, S. Hoeppener, I. Nischang, K. Sakurai, J. C. Brendel, *Macromolecules* **2020**, *53*, 7552–7560.

[32] N. Chebotareva, P. H. H. Bomans, P. M. Frederik, N. A. J. M. Sommerdijk, R. P. Sijbesma, *Chem. Commun.* **2005**, 4967–4969.

[33] J. Liu, M. J. G. Schotman, M. M. R. M. Hendrix, X. Lou, P. P. Marín San Román, I. K. Voets, R. P. Sijbesma, *J. Polym. Sci.* **2021**, *59*, 1162–1170.

[34] J. Liu, Y. Zhang, K. van Dongen, C. Kennedy, M. J. G. Schotman, P. P. Marín San Román, C. Storm, P. Y. W. Dankers, R. P. Sijbesma, *Biomacromolecules* **2023**, *24*, 2447–2458.

[35] S. Boileau, L. Bouteiller, F. Laupretre, F. Lortie, *New J. Chem.* **2000**, *24*, 845–848.

[36] L. Bouteiller, O. Colombani, F. Lortie, P. Terech, *J. Am. Chem. Soc.* **2005**, *127*, 8893–8898.

[37] O. Colombani, L. Bouteiller, *New J. Chem.* **2004**, *28*, 1373–1382.

[38] M. Roman, C. Cannizzo, T. Pinault, B. Isare, B. Andrioletti, P. van der Schoot, L. Bouteiller, *J. Am. Chem. Soc.* **2010**, *132*, 16818–16824.

[39] P. Ribagnac, C. Cannizzo, R. Meállet-Renault, G. Clavier, P. Audebert, L. Bouteiller, *J. Phys. Chem. B* **2013**, *117*, 1958–1966.

[40] E. Obert, M. Bellot, L. Bouteiller, F. Andrioletti, C. Lehen-Ferrenbach, F. Boué, *J. Am. Chem. Soc.* **2007**, *129*, 15601–15605.

[41] M. Tharcis, T. Breiner, J. Belleney, F. Boué, L. Bouteiller, *Polym. Chem.* **2012**, *3*, 3093–3099.

[42] F. Lortie, S. Boileau, L. Bouteiller, C. Chassenieux, B. Demé, G. Ducouret, M. Jalabert, F. Lauprêtre, P. Terech, *Langmuir* **2002**, *18*, 7218–7222.

[43] E. E. Dormidontova, *Macromolecules* **2004**, *37*, 7747–7761.

[44] L. Albertazzi, F. J. Martinez-Veracoechea, C. M. A. Leenders, I. K. Voets, D. Frenkel, E. W. Meijer, *Proc. Nat. Acad. Sci.* **2013**, *110*, 12203–12208.

[45] L. Su, J. Mosquera, M. F. J. Mabesoone, S. M. C. Schoenmakers, C. Muller, M. E. J. Vleugels, S. Dhiman, S. Wijker, A. R. A. Palmans, E. W. Meijer, *Science* **2022**, *377*, 213–218.

[46] R. P. M. Lafleur, S. Herziger, S. M. C. Schoenmakers, A. D. A. Keizer, J. Jahzerah, B. N. S. Thota, L. Su, P. H. H. Bomans, N. A. J. M. Sommerdijk, A. R. A. Palmans, R. Haag, H. Friedrich, C. Böttcher, E. W. Meijer, *J. Am. Chem. Soc.* **2020**, *142*, 17644–17652.

[47] J.-J. Max, C. Chapados, *J. Chem. Phys.* **2009**, *131*, 184505.

[48] M. C. A. Stuart, J. C. Van De Pas, J. B. F. N. Engberts, *J. Phys. Org. Chem.* **2005**, *18*, 929–934.

[49] R. P. M. Lafleur, S. M. C. Schoenmakers, P. Madhikar, D. Bochicchio, B. Baumeier, A. R. A. Palmans, G. M. Pavan, E. W. Meijer, *Macromolecules* **2019**, *52*, 3049–3055.

[50] S. Varela-Aramburu, G. Morgese, L. Su, S. M. C. Schoenmakers, M. Perrone, L. Leanza, C. Perego, G. M. Pavan, A. R. A. Palmans, E. W. Meijer, *Biomacromolecules* **2020**, *21*, 4105–4115.

[51] See Ref. [45].

[52] Anatrace, Handling and Storage of Polyethylene glycol Monoalkyl Ethers.

[53] See Ref. [42].

[54] J. Pérez-Folch, J. A. Subirana, J. Aymami, *J. Chem. Crystallogr.* **1997**, *27*, 367–369.

[55] See Ref. [40].